Combust. Sci. Tech., 1996, Vol. 115, pp. 151–176
Reprints available directly from the publisher
Photocopying permitted by license only

NO Production and Destruction in a Methane/Air Diffusion Flame

KERMIT C. SMYTH

Building and Fire Research Laboratory, National Institute of Standards and Technology, Gaithersburg, MD 20899

(Received 2 November 1995; in final form 14 February 1996)

Concentration profiles have been measured for naturally occurring NO in a laminar CH_4/air diffusion flame burning on a rectilinear Wolfhard-Parker slot burner at atmospheric pressure. Linear laser-induced fluorescence of the $A^2\Sigma^+$-$X^2\Pi_i$(0,0) transition was excited using a frequency doubled tunable dye laser and detected with a dielectric filter/photomultiplier tube combination. The observed fluorescence signals have been corrected for (1) the Boltzmann population in the $R_1(17)$ rotational level of the ground vibronic state and (2) collisional quenching rates as a function of the local temperature and collider concentrations. The resulting relative concentration profiles have been calibrated using tunable diode laser absorption measurements of Hill and Miller [1994]. Both the overall NO production/destruction rates and the contributions from individual elementary steps have been derived; the latter analysis utilizes previously measured profiles of H, O, OH, CH, and CH_3 as well as an estimated $^3CH_2$ profile.

The NO profile measurements alone do not distinguish its dominant production pathway in this co-flowing CH_4/air flame, since the contribution of prompt NO production is obscured by competing CH_i + NO destruction reactions. As a consequence of these reburn reactions, the observed peak NO concentrations are observed to closely track the maximum temperatures. A reaction path analysis and determination of NO fluxes strongly indicate that prompt NO production outweighs the thermal route, but uncertainities in determining the relative contributions to instantaneous NO production are large.

Keywords: Prompt NO; thermal NO; methane combustion; reburn chemistry; laminar diffusion flames; laser-induced fluorescence; rate analysis

1. INTRODUCTION

Nitric oxide is the most abundant NO_x species produced in combustion devices, yet the dominant route for its formation in hydrocarbon diffusion flames has not been established. Such flame systems are of particular interest from a practical viewpoint, and they exhibit significant differences in flame

structure compared to premixed flames. The extended high-temperature postflame region of premixed flames favors NO formation via the thermal (Zeldovich) mechanism, which involves the following reactions:

$$O + N_2 \rightarrow NO + N \tag{1}$$

$$N + O_2 \rightarrow NO + O \tag{2}$$

$$N + OH \rightarrow NO + H. \tag{3}$$

In diffusion flames the two primary contributions to NO formation are thought to arise [Drake and Blint, 1991a; Nishioka *et al.*, 1994] from this route and the prompt (Fenimore) mechanism, for which the reaction

$$CH + N_2 \rightarrow HCN + N \tag{4}$$

is usually invoked as the key step. In a modeling study of opposed flow CH_4/N_2/air diffusion flames, Drake and Blint [1991a] examined the relative importance of these two pathways and reactions involving N_2O. For all values of stretch, they found that the prompt mechanism made the largest contribution, followed by the thermal mechanism. Similar conclusions were reached in the modeling study of Nishioka *et al.* [1994]. However, direct experimental tests of these predictions have not been forthcoming. Drake and Blint [1991a] cite earlier work from their laboratory comparing CH_4 versus CO/H_2 fuels in counterflow diffusion flames which suggests that the Fenimore prompt mechanism contributes ~ 70% of the NO produced in their methane flame.

Although numerous prior investigators have reported NO concentration profiles in laminar premixed flames using both mass spectrometric sampling methods and laser-induced fluorescence, few such measurements have been made in hydrocarbon diffusion flames. Tuteja and Newhall [1972] measured NO concentrations in an axisymmetric, laminar CH_4/air diffusion flame by quartz microprobe sampling followed by a modified Saltzman analysis. Their NO profiles exhibit peak levels near 100 ppm (on a dry basis) at the location of the temperature maxima. No evidence for NO production from fuel derived species (i.e., prompt NO) was found. Mitchell *et al.* [1980] also employed microprobe sampling to measure NO and HCN concentrations in a similar axisymmetric CH_4/air diffusion flame. They found peak NO concentrations approaching 100 ppm (on a wet basis) and carried out a flux analysis. NO production both from the thermal route and from the oxidation of nitrogen-

containing species (specifically HCN) were identified, but no clear conclusion could be drawn concerning the dominant production pathway. Jaasma and Borman [1980] monitored NO in heptane flames and investigated the sensitivity of their chemiluminescence analyzer to hydrocarbon pyrolysis products. More recently, Sick and Lindstedt [1994] have reported initial results of a combined experimental/computational study of NO formation in counterflow CH_4/air diffusion flames. NO production from fuel nitrogen in diffusion flames has been investigated by Sarofim *et al.* [1975], Fenimore [1976], and Hahn and Wendt [1981] using gas sampling approaches. Turns [1995] has reviewed NO_x measurements and modeling investigations in laminar and turbulent diffusion flames.

This paper presents NO profile measurements in a well characterized CH_4/air diffusion flame burning at atmospheric pressure. Our detailed measurements of species concentrations, temperatures, and velocities [Smyth *et al.*, 1985; Norton *et al.*, 1993] constitute a comprehensive experimental database with which to examine NO formation and destruction routes. For example, overall net production/destruction profiles can be derived, as well as individual production and destruction rate profiles for specific elementary steps. Of particular importance for NO production, relative concentration profiles for O atom [Smyth and Tjossem, 1990] and CH [Norton and Smyth, 1991] have been previously measured, and peak concentrations for these radicals have been estimated. In addition, OH [Smyth *et al.*, 1990], H atom [Smyth and Tjossem, 1990], CH_3 [Smyth and Taylor, 1985; Miller and Taylor, 1987], and a derived $^3CH_2$ profile [Norton and Smyth, 1991] have been obtained. Using this body of information, one can evaluate the prompt and thermal contributions to NO production and also compare NO removal rates due to reactions with the radical pool species (H, O, and OH) versus CH_i species (CH, $^3CH_2$, and CH_3). These experimental results also serve as a useful test for models of the chemical structure of CH_4/air diffusion flames. Comparisons can be made either in terms of direct flame structure computations in the rectilinear Wolfhard-Parker geometry [Leung and Lindstedt, 1995] or for best matched mixture fraction and scalar dissipation rates independent of the burner geometry [Norton *et al.*, 1993].

2. EXPERIMENTAL APPROACH

The Wolfhard-Parker slot burner used in these experiments has been described in detail previously [Norton *et al.*, 1993 and references therein]. Figure 1 is a schematic diagram of this burner, the flame stabilizing screens,

and the optical setup. Flame conditions were identical to those used in prior profile measurements of the temperature, velocity, and species concentrations [Smyth *et al.*, 1985; Norton *et al.*, 1993]. Ultra high purity (99.9%) methane flows from the center 8 mm wide slot (cold flow velocity = 11.0 cm/s) and dry air from the outer two 16 mm slots (cold flow velocity = 21.7 cm/s), producing an overventilated diffusion flame with two identical, two-dimensional flame sheets. A long pathlength (40–45 mm) of uniform temperature and chemical composition along the direction of the laser beam renders this geometry especially well suited for laser-induced fluorescence measurements. Symmetry about the burner centerline allows highly precise lateral profile measurements to be made ($\pm$ 0.1 mm in the x direction, Fig. 1).

Laser-induced fluorescence from the (0,0) band in the $A^2\Sigma^+ - X^2\Pi_i$ transition of NO was excited in a one-photon process at $\sim$ 226 nm using a 10 Hz Continuum Surelite Nd^{3+}:YAG laser * to pump a Lumonics HD-500 tunable dye laser, followed by frequency doubling with a beta-barium borate crystal. The low concentrations of naturally occurring NO led to relatively weak

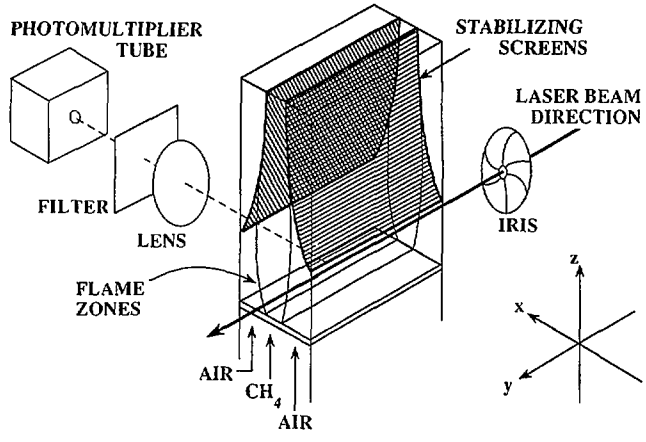

FIGURE 1 Schematic diagram of the co-flowing Wolfhard-Parker slot burner for the atmospheric pressure CH_4/air diffusion flame and the optical setup for the laser-induced fluorescence measurements. The flame is stabilized by two curved screens, which serve as heat sinks for the high-temperature reaction zones at $\sim$45 mm above the burner surface (Smyth *et al.*, 1985).

*Certain trade names and company products are identified in the text in order to adequately specify the experimental procedure and equipment used. In no case does such identification imply recommendation or endorsement by the National Institute of Standards and Technology, nor does it imply that the products are necessarily the best available for the purpose.

fluorescence signals when the incoming laser beam was focussed with a lens to beam diameters of 100–200 μm. Since the NO profiles are broad and extend over a wide region of this CH_4/air diffusion flame, a larger beam diameter could be employed without loss of critical spatial information. The laser beam was simply passed through 1mm diameter pinholes in order to obtain an improved signal-to-noise ratio. Under these conditions, linear laser-induced fluorescence data were obtained with energies of 60–70 μJ/pulse, a laser bandwidth of 0.07 cm^{-1} for the frequency-doubled dye laser output, and a pulse duration of ~3–4 ns for the fundamental beam.

A photomultiplier tube detected the laser-induced fluorescence at 90° to the direction of the laser beam through a dielectric filter whose 25 nm bandpass (FWHM) was centered at 239 nm. This detection bandpass covers emission primarily from the (0,0), (0,1), and (0,2) vibrational bands of the NO $A^2\Sigma^+ - X^2\Pi_i$ transition [Pearse and Gaydon, 1976]. Broadband laser-induced fluorescence attributed to polycyclic aromatic hydrocarbons (PAH) is also readily excited at ultraviolet wavelengths [Smyth *et al.*, 1985]. For the present experiments this PAH fluorescence was an observable but relatively weak interference compared to the NO fluorescence signals (see Fig. 3, Results section). No interference from O_2 fluorescence [Wysong *et al.*, 1989; Battles and Hanson, 1995; Partridge *et al.*, 1995] was detected when exciting the $R_1(17)$ and $Q_1(28)$ transitions at 225.47 nm and 225.14 nm, respectively.

NO profiles were measured at 2mm increments for heights H of 3–11 mm above the burner surface by translating the burner perpendicular to the laser beam direction. Typically, these measurements involved averaging 20 laser shots per position and taking points every 0.2 mm in the x direction at the center plane perpendicular to the long axis of the burner (see Fig. 1). Laser energy readings were recorded simultaneously; both the NO and PAH fluorescence signals were linear with the beam intensity. Profile data were obtained with the laser wavelength tuned on and off resonance for NO fluorescence for each height in the flame and then subtracted. There was no observable attenuation of the incident laser beam nor trapping of the NO fluorescence.

3. RESULTS

Figure 2 presents a portion of the laser-induced $A^2\Sigma^+ \leftarrow X^2\Pi_i$ excitation spectrum for naturally occurring NO in the CH_4/air diffusion flame. The bandhead region for the (0,0) transition was assigned using the compilation of Engleman *et al.* [1970]; no interfering O_2 lines were present.

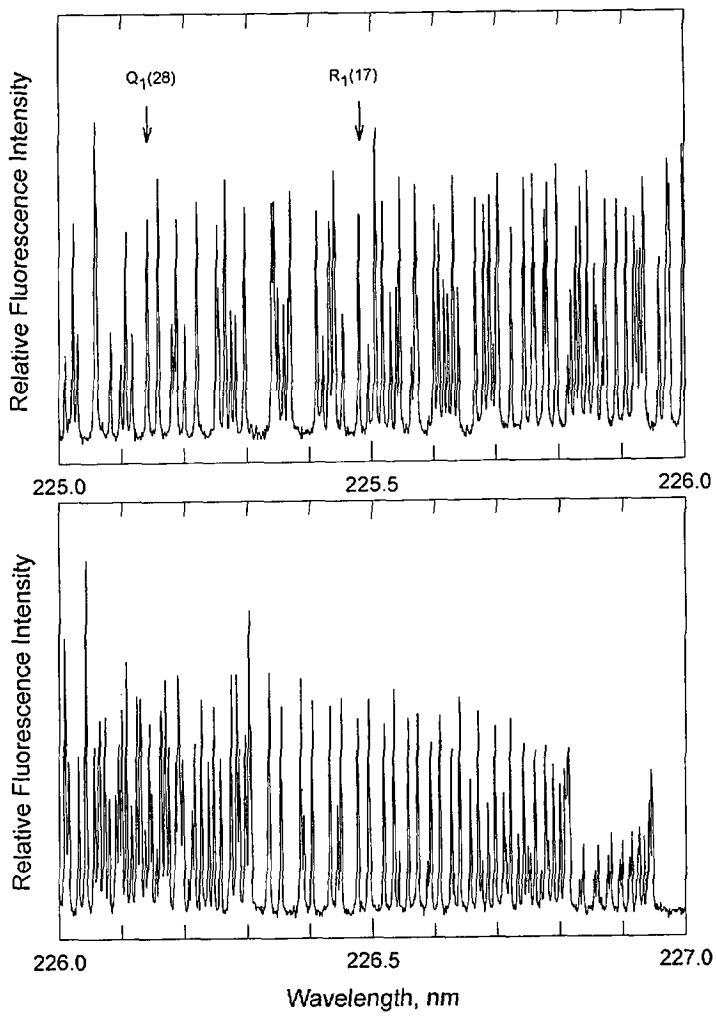

FIGURE 2 Laser-induced fluorescence spectrum of nascent NO measured 4 mm above the burner in the CH_4/air diffusion flame. The (0,0) band of the $A^2\Sigma^+ - X^2\Pi_i$ transition is excited, and the fluorescence emission from the (0,0), (0,1), and (0,2) bands is detected using a dielectric filter/photomultiplier tube combination. Arrows indicate the $R_1(17)$ and $Q_1(28)$ rotational lines used in the profile measurements.

Prior investigators have selected a variety of initial rotational lines for making NO fluorescence measurements. This is facilitated by the open nature of the NO electronic spectrum, which offers numerous isolated lines. Since NO is relatively unreactive, laser-induced fluorescence signals are observed throughout the diffusion flame from the peak temperature regions to the centerline, for example, over

a temperature range of 550–2080 K at a height of $H = 9$ mm above the burner. Using a temperature of 1900 K to characterize the high-temperature reaction zone, the maximum NO population in a rotational level occurs for $N'' = 19$, while the level least sensitive to temperature is $N'' = 28$. In the present study measurements were made for the isolated $R_1(17)$ and $Q_1(28)$ lines. It was initially thought that the $Q_1(28)$ transition would be preferable, since the Boltzmann population for this level varies slowly in the flame region where NO production and destruction occur ($T \sim$ 1400–2100 K). Thus, corrections for the Boltzmann population are small in the high-temperature reaction zones for this rotational line. However, the $R_1(17)$ transition gave superior profiles in terms of signal-to-noise. Both sets of data were analyzed to give a net NO production/destruction rate profile (see next section) and yielded identical results.

Determination of relative concentration profiles (either in terms of the number density or the mole fraction) from the observed laser-induced fluorescence signals requires corrections for (1) the variation of the Boltzmann population of the rotational level initially excited due to differing flame temperatures and (2) the variation of the collisional quenching rate with flame position due to changes in the local temperature and collider concentrations. Since the temperature field is known to within $\pm$ 5% in this flame [Smyth *et al.*, 1985; 1990], corrections for the relative Boltzmann population as a function of spatial location are straightforward. Quantitative quenching rates were computed from the known temperatures and the major species concentrations [Norton *et al.*, 1993] using the extensive data and correlations from Paul *et al.* [1994] and Furlanetto *et al.* [1994]. Figure 3 presents raw profile data for the NO laser-induced fluorescence measurements, as well as the Boltzmann fraction and collisional quenching rate corrections as functions of lateral position. The on-resonance profile shows the extended region over which NO fluorescence is detected, while the off-resonance data reveal weak contributions from both Rayleigh scattering and broadband molecular fluorescence.

A possible concern in making laser-induced fluorescence profile measurements in diffusion flames, where steep gradients of temperature and species concentrations exist, is that the NO absorption lineshape may vary significantly as a function of spatial location due to changes in the local temperature and collisional environment. For example, the centerline intensity for a given ro-vibronic transition decreases as the lineshape broadens for the same integrated overall intensity. This will be evident only for conditions where the laser bandwidth is considerably narrower than the NO linewidth. Our Lumonics dye laser has a narrow bandwidth in the frequency-doubled beam, $\sim$ 0.07 cm^{-1} at 226 nm, compared to the measured NO linewidth of 0.45–0.51 cm^{-1} in this flame. In addition to collisional and Doppler broadening

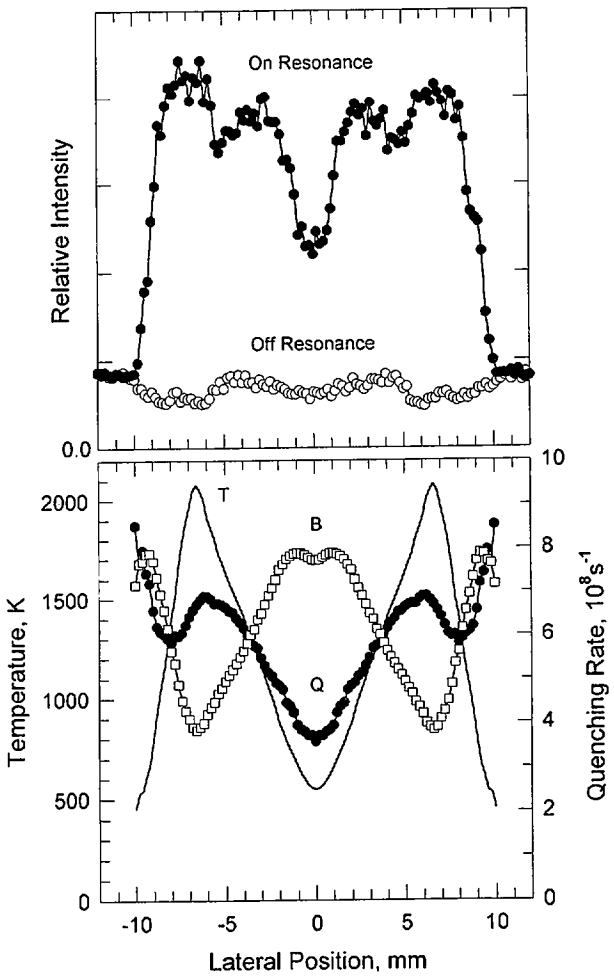

FIGURE 3 Top: On resonance NO laser-induced fluorescence signal for excitation of the $R_1(17)$ line at $H = 9$ mm above the burner surface (filled circles) and off-resonance profile (open circles); the original data are shown. Bottom: Temperature (T, solid line, maximum = 2080 K), the relative Boltzmann population (B, open squares, arbitrary scaling), and the calculated quenching rate (Q, filled circles) as a function of lateral position at the same height. These profiles have been averaged about the burner centerline, and the zero position is the same for all three curves. The peak value of the rotational partition function for the $N'' = 17$ level of the F_1 component is 2.25% at $x = \pm 1.0$ and ± 9.2 mm.

considerations, small lineshifts can occur for different temperatures and collider environments [Chang *et al.*, 1992; Carter and Barlow, 1994]. To address these considerations, lineshape measurements were made for excitation of the $R_1(17)$ line at several lateral positions which span the NO production/destruc-

tion region ($x = 4.0$–8.0 mm at $H = 9$ mm above the burner surface; $T = 1415$–2080 K; see Fig. 1 and the next section). No discernible variation in lineshape was observable, nor were lineshifts detected. Carter and Barlow [1994] reported similar results in H_2/air flames, wherein corrections for line broadening were required only for temperatures below 1000 K. At the centerline of our CH_4/air flame for $H = 9$ mm above the burner, where the mole fraction of methane is 0.79 and the temperature is 550 K, the observed NO lineshape was observed to be slightly broader (by $\sim 13\%$) and red-shifted. However, at this location the low temperature environment is chemically unreactive. Profile measurements were also made for a broader laser bandwidth of 0.14 cm^{-1} for the frequency-doubled beam; the shapes of the NO profiles were found to be identical to those measured with a bandwidth of 0.07 cm^{-1}. Based upon these results, no lineshape or lineshift corrections were required for the NO profiles obtained with narrow laser bandwidth excitation.

The relative NO concentration profiles measured in the present investigation have been placed on an absolute basis by comparison with recent tunable diode laser absorption measurements in an identical CH_4/air diffusion flame [Hill and Miller, 1994]. These infrared data exhibit maximum NO concentrations in the range of 30–53 ppm for heights of 3–11 mm above the Wolfhard-Parker burner surface. The calibration point selected is at the midpoint of this range ($H = 7$ mm), where the measured peak NO mole fraction is 46 ppm, with an estimated uncertainty of $\pm 20\%$.

Figure 4 presents the resulting quantitative NO concentration profiles for $H = 3$–11 mm above the burner surface (note the offset of 10 ppm for each profile). The most interesting aspects of these measurements are (1) the maximum NO concentration increases only slowly (37–49 ppm) with height, and (2) the peak NO concentrations consistently follow the temperature maxima (2013 K at $H = 3$ mm, $x = \pm 5.8$ mm; 2049 K at $H = 5$ mm, $x = \pm 6.2$ mm; 2051 K at $H = 7$ mm, $x = \pm 6.4$ mm; 2080 K at $H = 9$ mm, $x = \pm 6.6$ mm; and 2100 K at $H = 11$ mm, $x = \pm 6.8$ mm). Similar observations have been reported for co-flowing axisymmetric CH_4/air diffusion flames by Tuteja and Newhall [1972] and Mitchell *et al.* [1980].

4. CHEMICAL RATE ANALYSIS

Information on the rates of chemical reactions involving NO can be extracted from an analysis of the concentration profile data presented above. In the following sections the net chemical production/destruction rate of NO is calculated using the NO mole fraction profiles, and the instantaneous rates of individual NO production and destruction reactions are estimated. Consider-

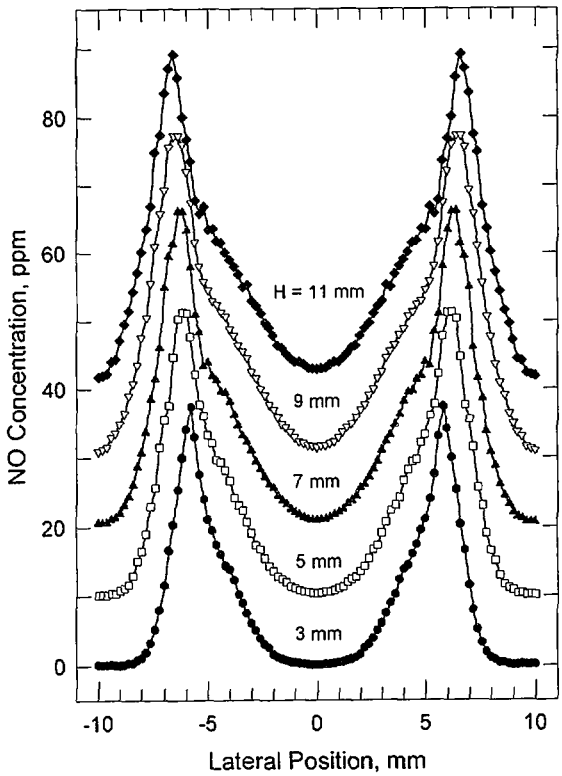

FIGURE 4 Quantitative NO concentration profiles at $H = 3$–11 mm above the burner surface; the data have been averaged about the burner centerline. Profiles at $H = 5, 7, 9$, and 11 mm have been offset by 10, 20, 30, and 40 ppm for clarity, respectively.

able attention has been devoted to developing a consistent set of temperature, velocity, and species concentration data for this CH_4/air flame [Norton *et al.*, 1993]. The following analysis centers on the region around $H = 9$ mm above the burner surface. Here hydrocarbon concentrations are appreciable, but significant amounts of soot have not yet formed [Smyth *et al.*, 1985]. Similar examinations of production and destruction rates have been performed previously in this flame for acetylene [Miller *et al.*, 1986; Smyth and Miller, 1987], CH_3 [Miller and Taylor, 1987], OH [Smyth *et al.*, 1990], and CH [Norton and Smyth, 1991].

4.1. Net NO Production/Destruction Rate

In a steady-state laminar diffusion flame, the net production or destruction rate of any species due to chemical reactions (R_i) must exactly balance the

divergence of the net flux of that species due to convective and diffusional transport at each flame location. Therefore, R_i can be calculated from the temperatures, velocities, and major species concentrations that have been measured in this flame [Smyth *et al.*, 1985; 1990]. The species conservation equation may be written [Miller *et al.*, 1986; Smyth and Miller, 1987] as

$$R_i = \nabla \cdot [N_i(\mathbf{v} + \mathbf{V}_i)], \tag{5}$$

where N_i is the concentration of species i, $\mathbf{v}$ is the bulk convective velocity, and $\mathbf{V}_i$ is the net diffusion velocity of species i into the local mixture. The calculation of R_{NO} was performed following the method of Miller *et al.* [1986]. Species concentration, velocity, and temperature data obtained at $H = 7, 9$, and 11 mm were used to compute derivatives in the vertical (z) direction. An effective multicomponent diffusion coefficient for NO into the local mixture was calculated as a combination of binary diffusion coefficients for NO in N_2, O_2, CH_4, H_2O, CO_2, H_2, CO, and C_2H_2 [Miller *et al.*, 1986].

Figure 5 presents the net production/destruction rate profile for NO at $H = 9$ mm above the burner surface. Two prominent features are evident: (1) a production peak located at ± 6.6 mm from the burner centerline, which coincides with the location of the temperature maximum of 2080 K; and (2) a destruction feature at ± 5.6 mm, close to the location of the peak CH concentration at ± 5.8 mm [Norton and Smyth, 1991]. Figure 5 also shows the temperature profile at $H = 9$ mm, along with the previously measured O atom [Smyth and Tjossem, 1990] and CH [Norton and Smyth, 1991] profiles. Note that the tail extending into the rich flame region in the O-atom profile is an experimental artifact, arising from the photolytic production of oxygen atoms [Smyth and Tjossem, 1990; Norton *et al.*, 1993]. It is tempting to associate the net NO production peak with the thermal pathway due to its close spatial proximity to the O-atom peak, while attributing NO destruction to reactions with CH_i species. Note that there is no direct evidence from either the NO profiles (Fig. 4) or the overall production/destruction rate profile (Fig. 5) that prompt NO production is occurring.

Experimental NO production/destruction rate profiles were also examined at $H = 5$ and 7 mm above the burner. These again show a single production peak at the location of the temperature maximum, whose magnitude is somewhat larger (by 30–40%) than that found at $H = 9$ mm, and a single destruction feature at richer flame positions of similar magnitude to that observed at $H = 9$ mm. Despite the fact that the peak CH concentration is significantly larger at lower flame heights [Norton and Smyth, 1991], there is

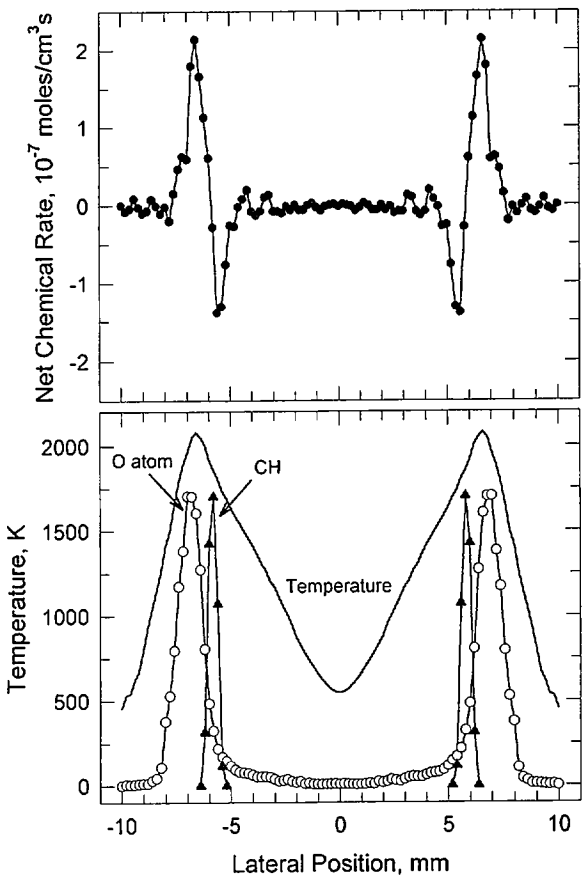

FIGURE 5 Top: Net rate of production and destruction of NO due to chemical reactions as a function of lateral flame position at $H = 9$ mm above the burner. The peak NO concentration at this height is 47 ppm. Positive values indicate net NO formation, and negative values denote net consumption. Bottom: Temperature (solid line, maximum = 2080 K), O-atom (open circles), and CH (filled triangles) profiles at $H = 9$ mm scaled to the same relative peak value.

no clear contribution of the prompt mechanism to these overall NO production rate profiles at the lower heights (and thus earlier times) in this flame. Neither the location of the maximum NO concentration nor the position of the net NO production feature shifts towards the rich flame region close to the burner surface.

4.2. Individual NO Production and Destruction Reactions

Since species concentration profiles for several key radicals have also been obtained in this CH_4/air diffusion flame, it is possible to assess the contribu-

tions of many individual reaction rates to the net chemical production/destruction rate profile for NO shown in Figure 5. In order to ascertain the relative contributions of various production and destruction pathways, it is necessary to measure or estimate peak radical concentrations. Our ability to do this for OH, H, O, CH, $^3CH_2$, and CH_3 is summarized below.

OH This is the best characterized radical in the CH_4/air diffusion flame. Absolute concentrations have been measured with an estimated accuracy of $\pm$ 10% over a dynamic range of ten [Smyth *et al.*, 1990]. The flame structure calculations of Smooke [Norton *et al.*, 1993] are in quantitative agreement with the measured superequilibrium peak mole fraction of 5.0×10^{-3} at $H = 9$ mm above the burner surface. Leung and Lindstedt [1995] calculate a somewhat higher mole fraction of 6.8×10^{-3}.

H Relative concentration profile measurements [Smyth and Tjossem, 1990] have been scaled to a peak mole fraction of 2.5×10^{-3}, based upon a partial equilibrium analysis [Smyth *et al.*, 1990]. The flame structure calculations of Smooke [Norton *et al.*, 1993] agree closely with this result, which is approximately 20 times higher than the full equilibrium value. Leung and Lindstedt [1995] report a slightly higher mole fraction of 3.3×10^{-3}.

O Only relative concentration profile measurements have been made [Smyth and Tjossem, 1990]. The shape and location of the O-atom profile in terms of mixture fraction are in good agreement with the flame structure calculations of Smooke [Norton *et al.*, 1993], except for the experimental tail into the rich flame region mentioned above. On the basis of this agreement, the peak O-atom mole fraction is scaled to the calculated value of 2.0×10^{-3} [Norton *et al.*, 1993], which is also the same peak concentration computed by Leung and Lindstedt [1995].

No quantitative concentration measurements have been reported for the CH_i radicals in a CH_4/air diffusion flame. In addition, considerable uncertainty exists in the reported rate constants for reactions which produce and destroy these species [Norton and Smyth, 1991; Etzkorn *et al.*, 1992; Williams and Fleming, 1994], and so establishing a consistent set of peak concentrations is much more difficult than for the major radical pool species discussed above. Flame structure computations are currently our best estimates, but these can be used only as a rough guide.

CH Relative concentration profile measurements have been made [Norton and Smyth, 1991]. The peak concentration is set to 0.7 ppm based upon the flame structure calculation of Smooke [Norton *et al.*, 1993].

$^3CH_2$ No experimental measurements of this species have been reported in any diffusion flame. Since reactions of triplet methylene with OH and H atom are thought to be the only significant sources of CH in this CH_4/air flame [Miller and Bowman, 1989], it is possible to derive a relative mole fraction profile for $^3CH_2$ [Norton and Smyth, 1991]. The peak concentration is set to the calculated value of 17.2 ppm [Norton *et al.*, 1993].

CH_3 Experimental profile measurements have been reported using multiphoton ionization to give relative concentrations [Smyth and Taylor, 1985] and quartz microprobe scavenger sampling experiments in which I_2 was added and CH_3I concentrations were measured [Miller and Taylor, 1987]. These two sets of profile data are in good agreement in terms of their location and their profile shapes [Norton *et al.*, 1993]. Lower bound estimates of the peak methyl radical mole fraction of 4.7×10^{-4} and 9.5×10^{-5} at $H = 9$ mm above the burner have been made from methyl radical recombination to produce C_2H_6 [Smyth and Taylor, 1985] and from the I_2 scavenging experiments [Miller and Taylor, 1987], respectively. These values are much lower than the flame structure computation of Smooke, wherein the peak methyl radical mole fraction is 2.3×10^{-3} [Norton *et al.*, 1993]. This computed peak concentration is used in the rate analysis to follow. Leung and Lindstedt [1995] calculated a smaller peak CH_3 mole fraction of 1.3×10^{-3}.

In addition to these CH_i radicals, calculations on premixed flames [Glarborg *et al.*, 1992; Lindstedt *et al.*, 1995] show that C, N, HCO, $^1CH_2$, HCCO, and CH_3O also react with NO and sometimes make the dominant contribution to NO removal [Lindstedt *et al.*, 1995]. However, no profile measurements of these species have been obtained in the CH_4/air diffusion flame, and so their possible contributions to NO consumption cannot be assessed from an experimental viewpoint.

Table I lists recommended rate constants for NO production and removal reactions. These values have been used as part of the basis for a methane combustion mechanism which includes nitrogen chemistry [GRI-MECH 2.11, 1995]. Figure 6 presents the instantaneous contributions of several individual reactions at $H = 9$ mm above the burner surface for the forward rates as given in Table I; note the different ordinate scales.

In Figure 6a the NO production profiles for the rate limiting steps involving the thermal (Reaction 1, see Introduction) and prompt (Reaction 4) pathways are plotted. Here the $O + N_2$ reaction rate has been multiplied by 2 to account

TABLE I NO Production and Destruction Rate Parameters, $k = A\,T^n \exp(-E_a/RT)$; units of cal, mole, cm^3, s, K

Reaction	*A*	*n*	E_a	*Reference*
Rate limiting reactions forming NO				
$O + N_2 \rightarrow NO + N$	1.05E14	0.0	75370	ML, DH
$CH + N_2 \rightarrow HCN + N$	4.00E08	1.1	20400	RS
Reactions consuming NO				
$NO + OH \rightarrow NO_2 + H$	3.66E09	0.8	28780	KF
$\rightarrow NH + O_2$	5.08E05	1.5	54460	MM
$\rightarrow HNO + O$	6.00E12	0.0	52570	S
$NO + H \rightarrow N + OH$	3.67E14	0.0	49560	BD
$NO + O \rightarrow N + O_2$	5.31E11	0.0	38230	A
$NO + CH \rightarrow HCN + O$	5.00E13	0.0	0	BD
$\rightarrow NCO + H$	2.00E13	0.0	0	BD
$\rightarrow HCO + N$	3.00E13	0.0	0	BD
$NO + {}^3CH_2 \rightarrow HCN + OH$	2.90E14	−0.69	760	BD
$\rightarrow HNCO + H$	3.10E17	−1.38	1270	BD
$\rightarrow HCNO + H$	3.80E13	−0.36	580	BD
$NO + CH_3 \rightarrow HCN + H_2O$	9.60E13	0.0	28800	Y
$\rightarrow H_2CN + OH$	1.00E12	0.0	21750	Y

DH Davidson and Hanson (1990); ML Michael and Lim (1992); RS Rodgers and Smith (1995); KF Ko and Fontijn (1991); MM Miller and Melius (1992); S. Smith, private communication (1995); BD Bozzelli and Dean (1995); A Atkinson *et al.* (1989); Y Yang *et al.* (1993).

Note: GRI-MECH 2.11 optimization has yielded the following *A*-factor values:

$O + N_2 \rightarrow NO + N$ $A = 1.46E14$
$CH + N_2 \rightarrow HCN + N$ $A = 2.86E08$
$NO + H \rightarrow N + OH$ $A = 2.44E14$.

for the likely quantitative reaction of $N + O_2$ (Reaction 2) to give a second NO molecule in lean flame regions [Drake *et al.*, 1987]. The peak thermal rate calculated using the parameters in Table I (1.2×10^{-7} moles/cm^3s) is in fair agreement with the calculated overall production rate (2.1×10^{-7} moles/cm^3s; Fig. 5) and occurs at the same spatial location ($\pm$ 6.6 mm from the burner centerline). This calculated $O + N_2$ rate is 30% smaller than found with the rate constant employed by Miller and Bowman [1989], Drake and Blint [1989], and Glarborg *et al.* [1992] for the present flame conditions. {The optimized rate parameters for this reaction (see Table I) give a calculated rate in good agreement with that determined using the older recommended values.} Since the thermal route has a high activation energy (Table I), its peak

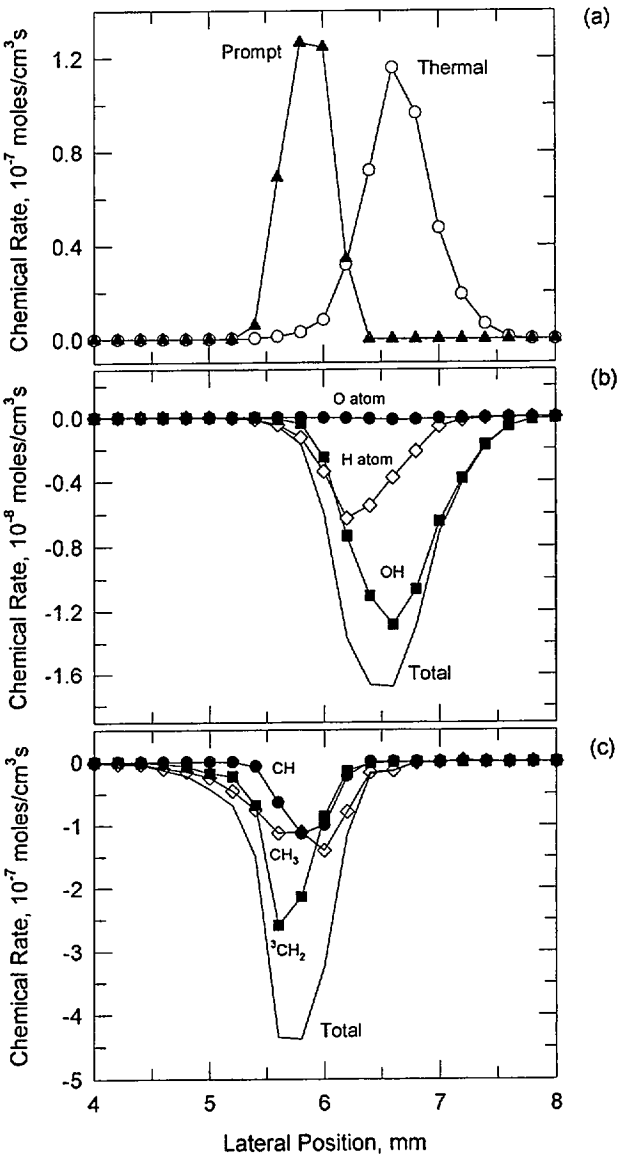

FIGURE 6 Individual contributions to NO production and destruction at $H = 9$ mm above the burner, based upon the rate constants listed in Table 1. The contribution for each reaction is shown for only the right-hand side of the flame. (a) NO production from the thermal (open circles) and prompt (filled triangles) pathways; (b) NO destruction by reactions with OH (filled squares), H atom (open diamonds), and O atom (filled circles), plus their sum (solid line); (c) NO destruction by reactions with CH (filled circles), $^3CH_2$ (filled squares), and CH_3 (open diamonds), plus their sum (solid line). Note the different ordinate scales in each panel.

rate occurs at the location of the maximum temperature, while for the prompt route the highest rate occurs at the position of the maximum CH concentration. Figure 6a shows that the calculated forward rate for $CH + N_2$ (1.3×10^{-7} moles/cm^{3}s) is close to that determined for $O + N_2$, using the rate parameters in Table I and the estimated peak CH concentration of 0.7 ppm. However, the uncertainty in the $CH + N_2$ rate constant is large. Using the rate constants from Miller and Bowman [1989] and Glarborg *et al.* [1992] gives a $CH + N_2$ rate ranging from $1.5–2.3 \times 10^{-7}$ moles/cm^{3}s, while the earlier values cited by Drake and Blint [1991b] yield rates from 0.97 to 3.4×10^{-7} moles/cm^{3}s. In addition, the calculated maximum CH concentration varies widely; Smooke obtains 0.7 ppm [the value used here; Norton *et al.*, 1993], whereas Leung and Lindstedt [1995] find 2.0 ppm.

Figures 6b and 6c plot the removal rates of NO by the major radical pool species (Fig. 6b) and by the CH_i radicals (Fig. 6c). The relative contributions of these reactions can be evaluated using the measured and estimated radical profiles and their peak concentrations, independent of the NO calibration. In Figure 6b the reaction with OH is fastest (giving over 98% $NO_2 + H$), followed by reaction with H atom, while the O-atom consumption route is negligible in this flame. As one would expect, these reactions occur in the high-temperature reaction zone, where the total estimated NO reactivity with the major radical pool species is 1.7×10^{-8} moles/cm^{3}s (for a peak NO concentration of 47 ppm at $H = 9$ mm above the burner). Since these reactions yield NO_2 and N atoms, both of which can react to produce NO, this removal rate does not constitute a net NO destruction rate.

Figure 6c presents estimated reaction rate profiles for NO with CH, $^3CH_2$, and CH_3. Although the uncertainties in the peak concentrations of these CH_i species are significant, as discussed above, it is evident that NO reacts much more rapidly with the CH_i radicals than with the major radical pool species (H, O, and OH). The fastest NO removal pathway involves triplet methylene, followed by comparable and significant contributions from CH and CH_3. The total removal rate of all the $NO + CH_i$ reactions is 4.4×10^{-7} moles/cm^{3}s, which is 26 times faster than the combined reactions of NO with OH, H, and O. This sum of individual NO consumption steps is also over three times greater than the measured net NO destruction feature (Fig. 5). Reactions of NO and the CH_i radicals occur for slightly rich conditions at a lateral location near $x = \pm 5.8$ mm. Here the local mixture fraction is 0.071, compared to the stoichiometric value of 0.055 [Norton *et al.*, 1993]. As is the case for NO reactions with the major radical pool species, each $NO + CH_i$ reaction yields a species (HCN, O, N) which may react to reform NO.

5. DISCUSSION

5.1. Net NO Production/Destruction Rate

The NO production/destruction rate profile shown in Figure 5 bears a close resemblance to the results of three computational investigations. In each case the calculated overall rate profile exhibits single production and destruction features, with destruction occurring at richer flame locations. The absolute magnitudes of these computed NO production and destruction rates are subject to large uncertainties, since the rate constants for several of the important reactions involving CH_i radicals are not well known. In addition, the absolute values in the experimental production/destruction rate profile are sensitive to the degree of data smoothing (see below). Nevertheless, it is instructive to examine the relative magnitudes and locations of the calculated production and destruction features compared to the experimental findings:

1. Drake and Blint [1989] presented an overall NO production/destruction rate profile in a counterflow $CO/H_2/N_2$ flame with a net production rate of $\sim 6 \times 10^{-8}$ moles/cm^{3}s and a net destruction rate of $\sim 3 \times 10^{-8}$ moles/cm^{3}s at a low strain rate of 0.1 s^{-1}. For this flame condition $[NO]_{max} = 2300$ ppm; note that the calculated production and destruction rates (moles/cm^{3}s) scale in direct proportion to the NO concentration. For a higher strain rate of 50 s^{-1} the peak NO concentration fell to ~ 50 ppm and only a much reduced net production peak was evident. In these computations only the thermal production route participates, and destruction occurs via reactions with the major radical pool species (H, O, and OH).

2. Drake and Blint [1991a] also investigated a counterflow CH_4/N_2 flame for a stretch of 42 s^{-1}. Here the overall computed production and destruction rates were considerably larger ($\sim 7 \times 10^{-7}$ and 4×10^{-7} moles/cm^{3}s, respectively, for $[NO]_{max} = 58$ ppm), and in addition the sums of all the individual production and all the individual destruction rates were approximately five times greater than those found in the $CO/H_2/N_2$ flame. The prompt NO production pathway dominates in this calculation, and NO destruction by reactions with CH_i species also occurs.

3. Nishioka *et al.* [1994] carried out computations of the chemical structure of a series of CH_4/air flames, including a counterflow diffusion flame. As found by Drake and Blint [1991a], they report that the Fenimore prompt route dominates NO production. Their overall production rate is $\sim 1.8 \times 10^{-6}$ moles/cm^{3}s, and the net NO destruction rate is $\sim 1.1 \times 10^{-6}$ moles/cm^{3}s for fuel and air velocities of 16 cm/s ($[NO]_{max} \sim 85$ ppm). Significant destruction was found only when the full mechanism was used, which included reactions with

CH_i species (specifically reactions 157–159 from the Miller-Bowman mechanism, 1989).

The present rate analysis of the NO profile measurements in the co-flowing CH_4/air flame gives peak production and destruction rates of 2.1×10^{-7} moles/cm^{3}s and 1.4×10^{-7} moles/cm^{3}s, respectively, at $H = 9$ mm above the burner surface (Fig. 5). The relative magnitudes of the experimental production and destruction features agree well with the computed values cited above. Absolute magnitudes in the determination of R_{NO} are sensitive to the degree of data smoothing, which is required before differentiation due to extreme sensitivity to noise [Eq. 5; Miller *et al.*, 1986]. Here the original NO fluorescence profile data have been smoothed twice with a 5-point Savitzky-Golay filter [Savitzky and Golay, 1964], which reduces the maximum values of NO production and destruction by 30–50%. Further smoothing with three passes reduces the peak values by only 7%. In addition, the 1 mm beam diameter used in the NO fluorescence measurements may also act to smooth the profile data somewhat and thereby reduce the absolute magnitudes in the derived production/destruction rate profile.

Both Drake and Blint [1991a] and Nishioka *et al.* [1994] clearly predict that the prompt route for NO production is much faster than the thermal mechanism and that reactions with CH_i species consume NO far more rapidly than do OH, H, and O. In contrast, neither the experimental NO profiles nor the overall production and destruction rate analysis provide sufficient information to identify the fastest NO formation pathway (see below). The experimental destruction feature does coincide with the spatial location of the CH_i radicals, which strongly suggests that these reburn reactions dominate NO consumption. Etzkorn *et al.* [1992] and Williams and Fleming [1994] have discussed the role of reburn chemistry in premixed methane flames, reaching quite different conclusions concerning how much seeded NO is consumed by these reactions. Sarofim *et al.* [1975] measured the recovery of NO added to the fuel stream of a confined CH_4/air diffusion flame and found that 74–83% of the seeded NO was consumed at an overall equivalence ratio of 1.0.

5.2. Individual NO Production and Destruction Reactions

The most dramatic result from the analysis of the individual contributions to the overall production and destruction of NO is that the NO + CH_i reactions are relatively fast and completely overwhelm production of NO by the prompt Fenimore mechanism. NO consumption and production processes which involve CH_i reactions occur at essentially the same spatial location in this

CH_4/air diffusion flame. These rapid consumption reactions help explain why the NO concentration profiles exhibit peak values at the temperature maxima. Furthermore, the reactions of NO with all of the CH_i radicals produce HCN (Table I), which can lead back to the formation of NO via the same pathway as in prompt NO production (Reaction 4). The key step in whether NO is actually removed or simply re-cyled involves the fate of the nitrogen atoms in HCN [Miller and Bowman, 1989]. N atoms can react with NO to form N_2 (reverse of Reaction 1) or with OH to yield NO (Reaction 3). Relative rates for these reactions have been determined using the present OH and NO profiles and rate parameters from GRI-MECH 2.11. The results of this analysis show that N atoms react with OH much more rapidly than with NO wherever OH is present (2–80 times faster, depending on the lateral position; $T = 1700$–2080 K at $H = 9$ mm above the burner). Only for temperatures below 1700 K, where N-atom concentrations are likely to be low, is NO actually destroyed. This situation greatly complicates assessing the relative contributions of the thermal and prompt pathways to overall NO production. A quantitative experimental profile of HCN in this flame, obtained for example using infrared absorption, would be valuable in determining the role of prompt NO formation and the overall rate of the CH_i reactions with NO.

Figure 6a suggests that the contributions from the thermal and prompt NO formation routes are roughly equal since the forward rates of $O + N_2$ and $CH + N_2$ are comparable (for the radical concentrations and rate constants selected here). However, another method to estimate the prompt contribution is to deduce the missing NO production feature which is offset by the combined CH_i + NO reburn reactions (Fig. 6c). This approach is illustrated in Figure 7, wherein all of the instantaneous removal rates plotted in Figure 6 are summed and compared to the experimentally derived NO production/destruction rate profile from Figure 5. In order to reconcile the total estimated instantaneous NO consumption rate with the net profile, the NO prompt production peak must be 4.1×10^{-7} moles/cm^{3}s at ± 5.8 mm, which is $\sim 2 \times$ larger than the thermal production peak (2.1×10^{-7} moles/cm^{3}s at ± 6.6 mm in Fig. 5). Thus, both NO production and consumption are expected to be most vigorous in a spatially narrow region just to the rich side of the maximum temperature location.

5.3. Flux Analysis

Since NO production and destruction have been examined only at early times in this CH_4/air flame, quantitative emission indices for the NO production pathways cannot be determined directly from these experimental measure-

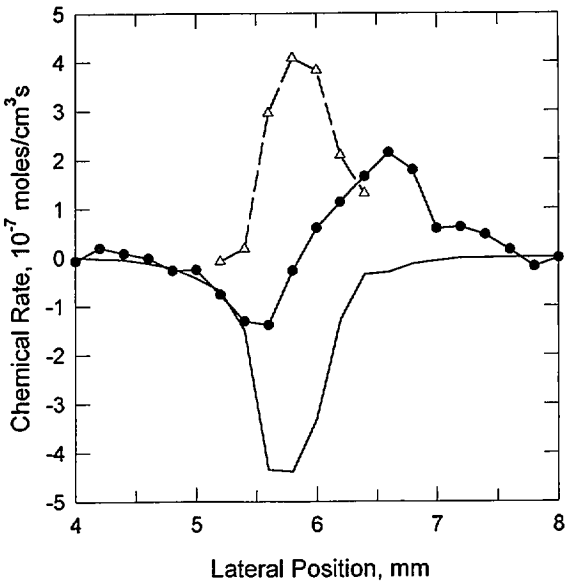

FIGURE 7 Comparison of the sum of all the instantaneous NO removal rates from Figure 6 (solid line) with the net chemical rate from Figure 5 (filled circles) results are presented only for a portion of the right-hand side of the flame. The derived instantaneous prompt NO production rate needed to reconcile these curves is shown as open triangles and a dotted line (see text).

ments. Mitchell *et al.* [1980] found that the thermal NO production route and the oxidation of nitrogen-containing species (especially HCN) made comparable contributions to NO emission. The modeling study of Nishioka *et al.* [1994] indicates that the thermal and prompt mechanisms contribute roughly equally to the NO emission index in a counterflow geometry; much faster prompt production is offset by CH_i + NO removal reactions.

The NO profiles in Figure 4 show that peak concentrations increase slowly (37–49 ppm for $H = 3$–11 mm) and the profile shape broadens somewhat with increasing height above the burner. This slow increase in the total integrated NO concentration indicates that NO is being consumed almost as fast as it is being produced. Figure 8 presents the results of a flux analysis, where the NO mass flux passing each measurement height H above the burner is given by

$$dm_{\mathrm{NO}(H)}/dt = L\int_{-\infty}^{\infty} Y_{\mathrm{NO}}(H,x)v_Z(H,x)dx.$$

Here L is the length of the flame sheets (4.1 cm along the y-direction in Fig. 1;

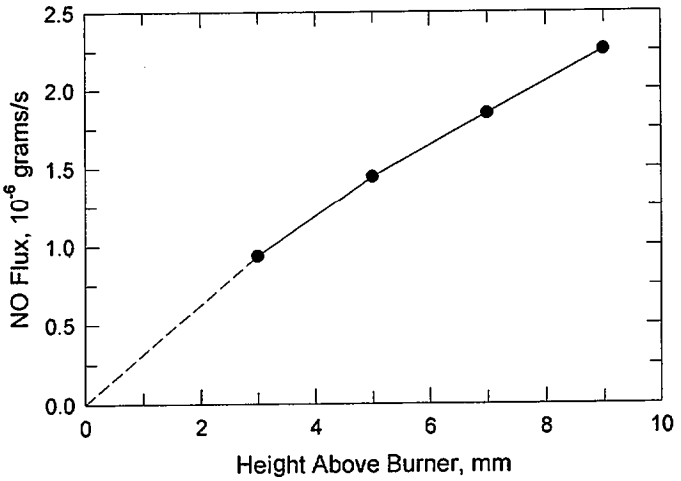

FIGURE 8 NO flux over the entire CH_4/air flame as a function of height above the burner. A dotted line is drawn from the lowest measurement height ($H = 3$ mm) to the burner surface.

Smyth *et al.*, 1990), $Y_{NO}(H, x)$ is the mass fraction of NO at a particular flame location, $v_z(H, x)$ is the vertical convective velocity, and dx is the distance between data points in the profile measurements (0.2 mm). Vertical diffusion velocities are estimated to be much smaller ($< 10\%$) than vertical convective velocities and have been neglected. The flux results reveal a steeper slope close to the burner surface (i.e., a more rapid overall rate of NO production), with a gradual decrease in net NO production with increasing height (and thus time) above the burner. This suggests that prompt NO production is more important close to the burner surface than at higher heights. To the degree that the rate limiting step for the prompt route is the $CH + N_2$ reaction, then prompt NO production is indeed expected to decrease with height above the burner because the CH concentration decreases steadily with increasing height over the range $H = 3$–13 mm [Norton and Smyth, 1991]. Note, however, that the methyl radical concentration profiles reveal no corresponding rapid reduction [Smyth and Taylor, 1985; Miller and Taylor, 1987; Norton *et al.*, 1993]. At $H = 9$ mm there is still ample methane to produce the CH_i radicals (the centerline CH_4 mole fraction is 0.79; Norton *et al.*, 1993), but increasing concentrations of stable hydrocarbons [Smyth *et al.*, 1985; Norton and Smyth, 1991] act as additional reaction sinks for CH. Throughout this region of the CH_4/air flame the thermal pathway makes a steady contribution to NO production; the rate of the $O + N_2$ reaction is estimated to increase by 28% with increasing height above the burner for $H = 7$–11 mm.

In summary, the experimental and computational studies of NO production in CH_4/air diffusion flames are in reasonable agreement, despite significant uncertainties in key radical concentrations and individual rate constants. At early times the instantaneous rate of prompt NO production is larger than the thermal route. However, overall NO production via the prompt mechanism is largely offset by fast $NO + CH_i$ consumption reactions. Both the prompt and thermal pathways contri-bute significantly to NO emission.

6. CONCLUSIONS

The goal of the current investigation was to evaluate the relative contributions of the thermal and prompt routes for NO production in a well characterized, laminar CH_4/air diffusion flame. This has proven to be elusive, despite having profile information on the H, O, OH, CH, $^3CH_2$, and CH_3 radicals. NO concentration profile measurements exhibit peak values at the local temperature maxima in this flame, coincident with the predicted peak rate for the thermal pathway. However, fast reburn reactions ($CH_i + NO$) completely offset the prompt NO production contribution in an overall production/destruction rate analysis. Examination of individual reaction steps and a flux analysis strongly suggest that the major contributor to instantaneous NO production involves the prompt mechanism, in agreement with model predictions. Quantification of the relative NO production contributions remains subject to large uncertainties in reported rate constants and in the estimation of radical concentrations.

Acknowledgements

This work has benefited greatly from many significant contributions. Joel Harrington carried out early spectroscopic work on NO, Dave Everest computed appropriate quenching rates for our flame system, Tom Norton helped clarify several kinetic questions, Tom Bowman provided recommended rate constants, Houston Miller and Deborah Hill furnished their quantitative NO profile data, and Chris Shaddix critically read the manuscript. Generous support is also acknowledged from the Basic Research Group of the Gas Research Institute, under Contract 5093-260-2676.

References

Atkinson, R., Baulch, D. L., Cox, R. A., Hampson, R.F. Jr., Kerr, J. A. and Troe, J. (1989). Evaluated Kinetic and Photochemical Data for Atmospheric Chemistry: Supplement III. *Journal of Physical and Chemical Reference Data*, **18**, 881.

Battles, B. E. and Hanson, R. K. (1995). Laser-Induced Fluorescence Measurements of NO and OH Mole Fraction in Fuel-Lean, High-Pressure (1–10 atm) Methane Flames: Fluorescence Modeling and Experimental Validation. *Journal of Quantitative Spectroscopy and Radiative Transfer*, **54**, 521.

Bozzelli, J. W. and Dean, A. M. (1995). Chapter on "Combustion Chemistry of Nitrogen" in *Combustion Chemistry*, Second edition, edited by W. C. Gardiner, Jr., Springer-Verlag, New York.

Carter, C. D. and Barlow, R. S. (1994). Simultaneous Measurements of NO, OH, and the Major Species in Turbulent Flames. *Optics Letters*, **19**, 299.

Chang, A. Y., DiRosa, M. D. and Hanson, R. K. (1992). Temperature Dependence of Collisional Broadening and Shift in the NO $A \leftarrow X(0, 0)$ Band in the Presence of Argon and Nitrogen. *Journal of Quantitative Spectroscopy and Radiative Transfer*, **47**, 375.

Davidson, D. F. and Hanson, R. K. (1990). High Temperature Reaction Rate Coefficients Derived From N-Atom ARAS Measurements and Excimer Photolysis of NO. *International Journal of Chemical Kinetics*, **22**, 843.

Drake, M. C., Correa, S. M., Pitz, R. W., Shyy, W. and Fenimore, C. P. (1987). Superequilibrium and Thermal Nitric Oxide Formation in Turbulent Diffusion Flames. *Combustion and Flame*, **69**, 347.

Drake, M. C. and Blint, R. J. (1989). Thermal NO_x in Stretched Laminar Opposed-Flow Diffusion Flames with $CO/H_2/N_2$ Fuel. *Combustion and Flame*, **76**, 151.

Drake, M. C. and Blint, R. J. (1991a). Relative Importance of Nitric Oxide Formation Mechanisms in Laminar Opposed-Flow Diffusion Flames. *Combustion and Flame*, **83**, 185.

Drake, M. C. and Blint, R. J. (1991b). Calculations of NO_x Formation Pathways in Propagating Laminar, High Pressure Premixed CH_4/Air Flames. *Combustion Science and Technology*, **75**, 261.

Engleman, R. Jr., Rouse, P. E., Peek, H. M. and Baiamonte, V. D. (1970). Beta and Gamma Band Systems of Nitric Oxide. Los Alamos Scientific Laboratory Report LA-4364.

Etzkorn, T., Muris, S., Wolfrum, J., Dembny, C., Bockhorn, H., Nelson, P. F., Attia-Shahin, A. and Warnatz, J. (1992). Destruction and Formation of NO in Low Pressure Stoichiometric CH_4/O_2 Flames. *Twenty-Fourth Symposium (International) on Combustion*, The Combustion Institute, Pittsburgh, PA, p. 925.

Fenimore, C. P. (1976). Effects of Diluents and Mixing on Nitric Oxide from Fuel Nitrogen Species in Diffusion Flames. *Sixteenth Symposium (International) on Combustion*, The Combustion Institute, Pittsburgh, PA, p. 1065.

Furlanetto, M. R., Thoman, J. W. Jr., Gray, J. A., Paul, P. H. and Durant, J. L. Jr. (1994). Near Resonant Electronic Energy Transfer in the Electronic Quenching of NO $A^2\Sigma^+$ by Hydrocarbons and Ammonia. *Journal of Chemical Physics*, **101**, 10452.

Glarborg, P., Lilleheie, N. I., Byggstøyl, Magnussen, B. F., Kilpinen, P. and Hupa, M. (1992). A Reduced Mechanism for Nitrogen Chemistry in Methane Combustion. *Twenty-Fourth Symposium (International) on Combustion*, The Combustion Institute, Pittsburgh, PA, p. 889.

GRI-MECH 2.11 (1995). Bowman, C. T., Frenklach, M., Gardiner, W. C. Jr. and Smith, G. P.; sponsored by the Gas Research Institute.

Hahn, W. A. and Wendt, J. O. L. (1981). NO_x Formation in Flat, Laminar Opposed Jet Methane Diffusion Flames. *Eighteenth Symposium (International) on Combustion*, The Combustion Institute, Pittsburgh, PA, p. 121.

Hill, D. A. and Miller, J. H. (1994). Measurement of Nitric Oxide in Probe-Extracted Combustion Gases Using Tunable Diode Laser Absorption Spectroscopy. Fall Technical Meeting of the Eastern States Section of the Combustion Institute (Clearwater, FL; December, 1994), p. 168.

Jaasma, D. and Borman, G. (1980). Peculiarities Associated with the Measurement of Oxides of Nitrogen Produced by Diffusion Flames. *Combustion Science and Technology*, **23**, 83.

Ko, T. and Fontijn, A. (1991). High-Temperature Photochemistry Kinetics Study of the Reaction $H + NO_2 \rightarrow OH + NO$ from 296 to 760 K. *Journal of Physical Chemistry*, **95**, 3984.

Leung, K. M. and Lindstedt, R. P. (1995). Detailed Kinetic Modeling of C_1-C_3 Alkane Diffusion Flames. *Combustion and Flame*, **102**, 129.

Lindstedt, R. P., Lockwood, F. C. and Selim, M. A. (1995). A Review of Detailed Kinetics of NO_x Formation and Removal in C/N/H/O System. Thermofluids Report TF/95/3, Mechanical Engineering Department, Imperial College.

Michael, J. V. and Lim, K. P. (1992). Rate Constants for the N_2O Reaction System: Thermal Decomposition of N_2O; $N + NO \rightarrow N_2 + O$; and Implications for $O + N_2 \rightarrow NO + N$. *Journal of Chemical Phy-sics*, **97**, 3228.

Miller, J. A. and Bowman, C. T. (1989). Mechanism and Modeling of Nitrogen Chemistry in Combustion. *Progress in Energy and Combustion Science*, **15**, 287.

Miller, J. A. and Melius, C. F. (1992). The Reactions of Imidogen with Nitric Oxide and Molecular Oxygen. *Twenty-Fourth Symposium (International) on Combustion*, The Combustion Institute, Pittsburgh, PA, p. 719.

Miller, J. H., Mallard, W. G. and Smyth, K. C. (1986). Chemical Production Rates of Intermediate Hydrocarbons in a Methane/Air Diffusion Flame. *Twenty-First Symposium (International) on Combustion*, The Combustion Institute, Pittsburgh, PA, p. 1057.

Miller, J. H. and Taylor, P. H. (1987). Methyl Radical Concentrations and Production Rates in a Laminar Methane/Air Diffusion Flame. *Combustion Science and Technology*, **52**, 139.

Mitchell, R. E., Sarofim, A. F. and Yu, R. (1980). Nitric Oxide and Hydrogen Cyanide Formation in Laminar Methane/Air Diffusion Flames. *Combustion Science and Technology*, **21**, 157.

Nishioka, M., Nakagawa, S., Ishikawa, Y. and Takeno, T. (1994). NO Emission Characteristics of Methane-Air Double Flame. *Combustion and Flame*, **98**, 127.

Norton, T. S. and Smyth, K. C. (1991). Laser-Induced Fluorescence of CH in a Laminar CH_4/Air Diffusion Flame: Implications for Diagnostic Measurements and Analysis of Chemical Rates. *Combustion Science and Technology*, **76**, 1.

Norton, T. S., Smyth, K. C., Miller, J. H. and Smooke, M. D. (1993). Comparison of Experimental vs. Computed Species Concentration and Temperature Profiles in Laminar, Two-Dimensional Methane/Air Diffusion Flames. *Combustion Science and Technology*, **90**, 1.

Partridge, W. P. Jr., Klassen, M. S., Thomsen, D. D. and Laurendeau, N. M. (1995). Experimental Assessment of O_2 Interferences on LIF Measurements of NO in Lean High-Pressure Premixed Flames Using Narrow-Band and Broad-Band Detection. Joint Technical Meeting of the Central and Western States (USA) Sections and the Mexican National Section of the Combustion Institute (San Antonio, TX; April, 1995), Paper 955-027, p. 139.

Paul, P. H., Carter, C. D, Gray, J. A., Durant, J. L. Jr., Thoman, J. W. and Furlanetto, M. R. (1994). Correlations for the NO $A^2\Sigma^+$ Electronic Quenching Cross-Section. Sandia Report SAND 94-8237.

Pearse, R. W. B. and Gaydon, A. G. (1976). *The Identification of Molecular Spectra*, Fourth Edition, Chapman and Hall, London.

Rodgers, A. S. and Smith, G. P. (1995). Pressure and Temperature Dependence of $CH + N_2$. Joint Technical Meeting of the Central and Western States (USA) Sections and the Mexican National Section of the Combustion Institute (San Antonio, TX; April, 1995), Paper 95S-042, p. 212.

Sarofim, A. F., Williams, G. C., Modell, M. and Slater, S. M. (1975). Conversion of Fuel Nitrogen to Nitric Oxide in Premixed and Diffusion Flames. *AIChE Symposium Series*, **71**, 51.

Savitzky, A. and Golay, M. J. E. (1964). Smoothing and Differentiation of Data by Simplified Least Squares Procedures. *Analytical Chemistry*, **36**, 1627.

Sick, V. and Lindstedt, R. P. (1994). The Formation and Destruction of Nitric Oxide in Laminar Counterflow Diffusion Flames. *Twenty-Fifth Symposium (International) on Combustion*, Work-in-Progress Poster # 4-75.

Smyth, K. C., Miller, J. H., Dorfman, R. C., Mallard, W. G. and Santoro, R. J. (1985). Soot Inception in a Methane/Air Diffusion Flame as Characterized by Detailed Species Profiles. *Combustion and Flame*, **62**, 157.

Smyth, K. C. and Miller, J. H. (1987). Chemistry of Molecular Growth Processes in Flames. *Science*, **236**, 1540.

Smyth, K. C. and Taylor, P. H. (1985). Detection of the Methyl Radical in a Methane/Air Diffusion Flame by Multiphoton Ionization Spectroscopy. *Chemical Physics Letters*, **122**, 518.

Smyth, K. C., Tjossem, P. J. H., Hamins, A. and Miller, J. H. (1990). Concentration Measurements of OH· and Equilibrium Analysis in a Laminar Methane/Air Diffusion Flame. *Combusion and Flame*, **79**, 366.

Smyth, K. C. and Tjossem, P. J. H. (1990). Relative H-Atom and O-Atom Concentration Measurements in a Laminar, Methane/Air Diffusion Flame. *Twenty-Third Symposium (International) on Combustion*, The Combustion Institute, Pittsburgh, PA, p. 1829.

Turns, S. R. (1995). Understanding NO_x Formation in Nonpremixed Flames: Experiments and Modeling. *Progress in Energy and Combustion Science* **21**, 361.

Tuteja, A. D. and Newhall, H. K. (1972). Nitric Oxide Formation in Laminar Diffusion Flames. Chapter in *Emissions from Continuous Combustion Systems*, W. Cornelius, Ed., Plenum, p. 109.

Williams, B. A. and Fleming, J. W. (1994). Comparative Species Concentrations in $CH_4/O_2/Ar$ Flames Doped with N_2O, NO, and NO_2. *Combustion and Flame*, **98**, 93.

Wysong, I. J., Jeffries, J. B. and Crosley, D. R. (1989). Laser-Induced Fluorescence of $O[3p^3P]$, O_2, and NO Near 226 nm: Photolytic Interferences and Simultaneous Excitation in Flames. *Optics Letters*, **14**, 767.

Yang, H., Lissianski, V., Okoroanyanwu, J. U., Gardiner, W. C. Jr. and Shin, K. S. (1993). Reaction Between CH_3 and NO at Combustion Temperatures. *Journal of Physical Chemistry*, **97**, 10042.